Bull. Soc. géol. Fr., 2003, t. 174, n° 1, pp. 45-57

The Hercynian collision in the Armorican Massif : evidence of different lithospheric domains inferred from seismic tomography and anisotropy

SÉBASTIEN JUDENHERC[1], MICHEL GRANET[1], JEAN-PIERRE BRUN[2] and GEORGES POUPINET[3]

Key words. – Hercynian collision, Armorican Massif, Seismictomography, Seismic anisotropy, Lithospheric domains.

Abstract. – The Hercynian belt is a continental collision orogen extending from south-west Iberia to the Bohemian Massif in Czech Republic. The successive stages of its formation are dated from 400 to 260 Ma.The Armorican Massif is a preserved segment of this orogen. It presents structures oriented NW-SE, parallel to the general Hercynian trend in this region. The massif is divided into three domains (North, Central, and South-Armorican domains) separated by two main shearzones, the North- and South-Armorican shear zones. As the Armorican Massif escaped from any important tectonic or thermal event since the end of Hercynian times, it is particularly suited for the study of an old collision orogen. Thus, in the framework of the GéoFrance3D-ARMOR2 project, two passive seismological experiments were conducted in 1997 and 1999 in the Armorican Massif. The main goals concerned the characterization of the deep geometry of both shear zones, the understanding of their geodynamic bearing on the long term evolution of the Hercynian belt, the study of the lithospheric deformation, and the 3D imaging of the Champtoceaux nappes.The data allow to model seismic anisotropy and to build a *3D P*-wave velocity model beneath the Armorican Massif. Crustal images do not evidence any deep rooting of the Champtoceaux nappes in the lower crust. However, the upper mantle images show a clear signal interpreted as the relic of the northward subduction which lasted until Devonian (≈ 350 Ma). The results also show that the North-Armorican Shear Zone is limited at depth to the crust and topmost mantle, while the South-Armorican Shear Zone can be traced over the whole lithosphere.The strong velocity contrasts are associated to probable relic thermal anomalies but are also significantly related to chemical anomalies.

La collision hercynienne dans le Massif armoricain : mise en évidence d'une différentiation lithosphérique à partir de la tomographie et de l'anisotropie sismiques

Mots clés. – Collision hercynienne, Massif armoricain, Tomographie sismique, Anisotropie sismique, Domaines lithosphériques.

Résumé. – La chaîne hercynienne est un objet majeur en Europe. Elle résulte de la collision de deux blocs continentaux durant le Paléozoïque. Le Massif armoricain présente l'intérêt de n'avoir été affecté par aucun événement tectonique ou thermique majeur depuis la fin de la collision (≈ 260 Ma). Nous y avons donc l'opportunité d'étudier la structure profonde d'une ancienne chaîne de collision. Les principaux traits géologiques du Massif armoricain sont les zones de cisaillement nord- et sud-armoricaines, orientée respectivement E-W et NW-SE. Elles séparent le massif en trois domaines : les domaines nord-, centre- et sud-armoricain.

Dans le but d'étudier la structure profonde de cette région, des réseaux sismologiques temporaires ont été installés en 1997 et 1999 dans le cadre du volet sismologique du projet ARMOR2-GéoFrance3D. Les stations temporaires, complétées par les sites permanents forment un réseau bidimensionnel dense de 80 stations couvrant une grande partie du Massif armoricain. Les données collectées durant ces expériences sont exploitées sous la forme d'un ensemble de temps d'arrivées d'ondes *P* et de formes d'ondes *S* télésismiques. Les méthodes utilisées pour l'imagerie du manteau supérieur sous le Massif armoricain consistent en la modélisation des variations de vitesse des ondes *P* et de l'anisotropie sismique. La tomographie de vitesse sismique est probablement l'outil le plus performant pour étudier l'intérieur de la Terre. Elle fournit des images structurales des régions étudiées sous la forme de perturbations de vitesse sismique qui représentent les effets de perturbations thermiques et/ou minéralogiques des milieux. Les études de laboratoire et les modélisations numériques montrent enfin que l'anisotropie sismique des roches du manteau supérieur reflètent l'orientation préférentielle des réseaux cristallins des grains d'olivine, représentant elle-même la fabrique tectonique de la roche, témoin des déformations passées, anciennes ou récentes.

Un modèle de vitesse des ondes *P* a été calculé, il procure les images des perturbations de vitesse jusqu'à la profondeur de 200 km. Dans la partie supérieure, jusqu'à 130 km, les images sont dominées par des vitesses élevées dans les régions de l'ouest du massif et par des vitesses faibles dans les régions du sud et de l'est. Aucune structure superficielle n'est corrélée à la frontière N-S entre les anomalies dans la partie centrale du Massif armoricain. Dans la partie inférieure du modèle (130-200 km), on observe un brusque changement de l'organisation de l'image. Les perturbations de vitesse sont organisées selon trois zones allongées d'orientation NW-SE. Le domaine central, caractérisé par des vitesses élevées est séparé du domaine sud par une limite dont la localisation et l'orientation correspondent à celles de la Zone de cisaillement sud-armoricaine en surface. La limite nord du corps rapide central est localisée 50 à 70 km vers le nord et montre la même orientation. A toutes les profondeurs, on observe que le sud du Cisaillement sud-armoricain,

[1]Ecole et Observatoire des Sciences de la Terre, UMR 7516, Strasbourg, France.
[2]Géosciences Rennes UPR 4661, France.
[3]Laboratoire de Géophysique Interne et de Tectonophysique, UMR 5559, Grenoble, France.
Manuscrit déposé le 28 juin 2001 ; accepté après révision le 2 septembre 2002.

c'est-à-dire le domaine sud-armoricain, est caractérisé par des anomalies négatives. Le Cisaillement nord-armoricain ne montre aucune corrélation avec le modèle de vitesse.

Au contraire, l'anisotropie des ondes P_n est fortement corrélée à la direction du Cisaillement sud-armoricain dans le sud du massif et à la direction du Cisaillement nord-armoricain dans le nord du massif. Cette corrélation n'est pas observée pour les onde *SKS* qui montrent une direction rapide NW-SE à travers tout le massif. Cependant, on distingue 2 groupes de mesures : au sud, le délai moyen est de 1,25 s alors qu'au nord, il est de 0,8 s. En supposant un taux d'anisotropie de l'ordre de 3 %, ces valeurs correspondent à des épaisseurs de l'ordre de 120 et 80 km, respectivement. De plus, une modélisation tridimensionnelle de la biréfringence des ondes *S* permet d'expliquer les données du nord du massif par un milieu à symétrie hexagonale dont le plan de symétrie (la fabrique) est incliné vers le SW. Dans le sud du massif, un plan de symétrie vertical satisfait les observations.

Ces résultats montrent que l'objet géologique majeur de cette région est le Cisaillement sud-armoricain dont on peut suivre la trace depuis la croûte jusqu'à la base du modèle à 200 km. Au contraire, le Cisaillement nord-armoricain semble affecter au plus le manteau sommital où se propagent les ondes P_n.

Les contrastes de vitesse sont assez élevés : plus de 5 % sur des distances de l'ordre de 30 km. Ces perturbations de vitesse sont associées au dernier événement tectonique majeur, la collision hercynienne qui s'est terminée il y a plus de 250 Ma. Dans ce cas, ces variations de vitesse sismique ne peuvent être expliquées exclusivement par des anomalies thermiques. Il est nécessaire de considérer une contribution minéralogique forte.

Les images tomographiques et les mesures d'anisotropie sont interprétées comme la conséquence d'un assemblage de deux lithosphères dont les origines sont différentes. Dans le nord de la Bretagne, les perturbations mineures de la vitesse des ondes *P*, les délais faibles et la structure inclinée de la fabrique lithosphérique caractérisent une lithosphère affectée par des événements pré-hercyniens, probablement liés à l'orogène Cadomien (650-540 Ma).Dans le centre et le sud de la Bretagne, l'image tomographique est interprétée comme la signature de la subduction à vergence nord qui a eu lieu avant la collision continentale. Les vitesses sismiques élevées représentent alors probablement un bloc de lithosphère subductée. Enfin, l'anisotropie mesurée dans le sud du Massif armoricain est attribuée au régime transpressif intense du Carbonifère au niveau de la zone du Cisaillement sud-armoricain.

INTRODUCTION

The Hercynian belt is a continental collision orogen extending from south-west Iberia to the Bohemian Massif in Czech Republic. This Hercynian orogeny (400-260 Ma) is largely responsible for the present-day structure of the Armorican Massif, and strongly reworked earlier structures related to the Cadomian orogeny (650-540 Ma).

The Armorican Massif shows a general E-W structural pattern (fig. 1) characterized by three domains : the North-Armorican Domain, the Central-Armorican Domain, and the South-Armorican Domain. They are separated by two main dextral shear zones of Carboniferous age (≈ 350-300) : the North-Armorican Shear Zone, and the South-Armorican Shear Zone.

The North-Armorican Domain (NAD) is mainly formed by Precambrian units strongly deformed and metamorphosed by the Cadomian orogeny [Cogné and Wright, 1980]. This domain is characterized by volcanic arcs and back arc basin accreted between 650 and 580 Ma [Auvray, 1979 ; Graviou and Auvray, 1985]. These formations were later thrusted onto a sedimentary margin between 580 and 540 Ma [Brun *et al*., 1991]. Yet, during the Hercynian orogeny, the NAD did underwent only small deformations.

The Central-Armorican Domain (CAD) is separated from the NAD to the north by the North Armorican Shear Zone (NASZ), and limited to the south by the South Armorican Shear Zone (SASZ). Most of the CAD is formed by Paleozoic sedimentary units unconformably lying onto Brioverian sediments, whose age ranges from upper Neoproterozoic to Cambrien (≈ 600 Ma). The age and nature of the basement beneath the Brioverian sediments remains unknown, but it could be the result of accretionnary processes of volcanic arcs related to the Cadomian orogeny. Finally, the CAD underwent a general moderate dextral simple shear during the Carboniferous.

FIG. 1. – Major geological structures of the Armorican Massif [after Chantraine *et al*., 1996]. NASZ: North Armorican Shear Zone; SASZ: South Armorican Shear Zone; N/EFZ: Nort/Erdre Fault Zone.
FIG. 1. – *Structures géologiques majeures du Massif armoricain.* NASZ : *cisaillement nord-armoricain ;* SASZ : *cisaillement sud-armoricain ;* N/EFZ : *zone de faille de Nort/Erdre.*

At the scale of the CAD, the base of Ordovician deposits, which were never metamorphosed, is affected by low amplitude, large wave length folds of Carboniferous age. Consequently, the sedimentary deposits in the CAD did not undergo any thrusting, suggesting that the crust was not significantly thickened during the Hercynian collision. This is in strong contrast with the Champtoceaux Nappes located immediately to the south of the CAD where some rocks have recorded high pressure metamorphism (≈ 20 kbar) followed by a fast exhumation at the early stage of the colli-

sion [Guiraud *et al*., 1987]. Finally, it is important to notice that during the Carboniferous, the displacement along the NASZ did not exceed a few tens of kilometers whereas it reaches over 300 km along the SASZ [Balé and Brun, 1986].

The South-Armorican Domain (SAD) is made of metamorphic and plutonic rocks marked by several metamorphic events during the continental collision. Metamorphism evolved from high pressure conditions (≈ 20 kbar) from Devonian to Carboniferous, to medium pressure high temperature conditions (≈ 10 kbar, ≈ 700-800 °C) from Upper Carboniferous to Permian. The latter event is related to a stage of extension parallel to the direction of the range from Visean to Westphalian (330-300 Ma) [Gapais *et al*., 1983 ; Brown and Dallmeyer, 1996].

The earliest stages of subduction are best preserved in the South-Armorican Domain, with such remnants as the highly metamorphosed rocks (≈ 15-20 kbar, 400-500°C) of Champtoceaux (shaded area in figure 1), of Groix Island and Vendée [Ballèvre *et al*., 2000 ; Bosse *et al*., 2000].

Since the last extensional events taking place during Permian, the Armorican Massif did not record any significant tectonic or thermal event. The only remarkable event is a southward tilt of the western part of the Armorican Massif, emphasized by recent topographic levelling [Lenôtre *et al*., 1999] and river incision [Bonnet, 1998]. The thermal and tectonic post-Hercynian history is rather quiet as compared to the Massif Central which was strongly affected by late Tertiary volcanic events, or to the Vosges-Black Forest mountains affected by the opening of the Rhine-Graben. Moreover, considering the amount of geological data in this region, the Armorican Massif is obviously suited for the study of the long term evolution of the lithosphere-asthenosphere system in a continental collision zone.

In the framework of the GéoFrance3D-ARMOR2 project, some stations of the Lithoscope French pool were installed in 1997 and 1999 during two complementary experiments. Together with the permanent stations of the national observatories (Laboratoire de Détection Géophysique and Réseau National de Surveillance Sismique) the temporary stations were laid out for a dense 2D array covering the major tectonic features of the Armorican Massif : the North-Armorican Shear Zone, South-Armorican Shear Zone, and Champtoceaux Nappes (fig. 2).

The aim of the ARMOR2 seismological experiments was to explore the deep lithosphere of a region stabilized after being strongly affected by the collision of two continental blocks. In particular, the results from teleseismic *P*-wave tomography and P_n and *SKS* anisotropy modelling are used to understand the geodynamical events which lead to the formation of the Armorican Massif.

They allow to constrain the extension at depth and the geometry of the main shear zones, and to characterize the lithospheric fabric associated with the successive tectonic events recorded by the Armorican Massif. Besides, the array installed in the southeastern part of the massif was designed to study the possible rooting of the Champtoceaux Nappes.

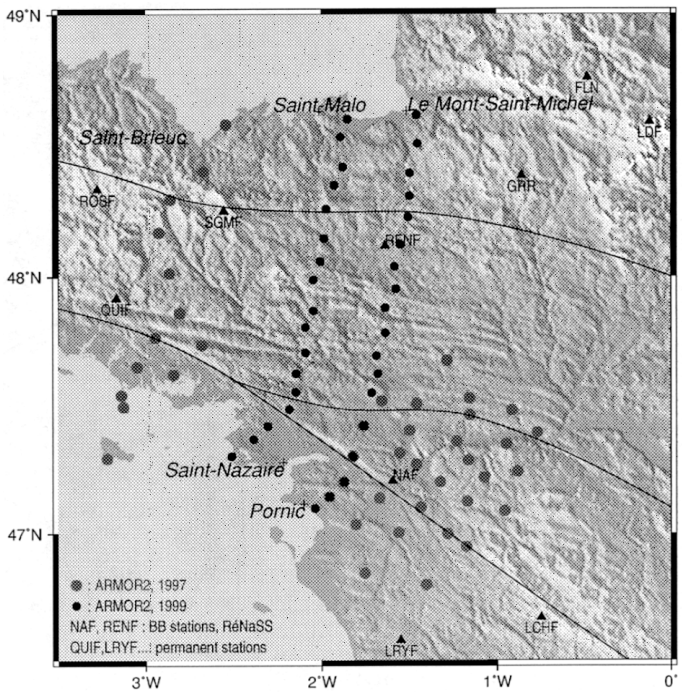

FIG. 2. – Map of the temporary stations installed in 1997 (small black circles) and 1999 (big circles).We represent the permanent stations belonging to the LDG (CEDA) and RéNaSS (INSU) networks which have been used in this work (black triangles).
FIG. 2. – *Carte des stations temporaires des expériences ARMOR2 1997 (petits disques noirs) et 1999 (grands disques). Les stations des réseaux permanents du LDG (CEA) et du RéNaSS (INSU)qui ont été utilisées sont représentées par des triangles.*

METHODS

Regional travel time tomography

Three-dimensionnal mapping of velocity variations provides information on the geometry of the structures in the lithosphere-asthenosphere system (LAS). In this study, we have used a linear approach of the teleseismic tomography problem. The region of interest is divided into constant thickness layers, each layer being divided into non overlapping blocks. Seismic velocity perturbations within each block are determined in order to explain the observed travel time perturbations (travel time residuals). Travel time residuals represent the difference between the observed travel time and a theoretical travel time computed assuming a 1D Earth model. This method is particularly suited for to regional scale problems, and was originally developped [Aki *et al*., 1977] with a simple ray tracing in the Earth model. The solution is usually obtained through a single linear inversion based on a damped least square approach [Franklin, 1970]. However, a three-dimensionnal ray tracing technique developed by Steck and Prothero [1991] was used in this work as a part of an iterative inversion process intended to take into account the non-linearity of the problem. Each step consists in solving a linear tomographic problem built on the ray geometry computed in the previous velocity model. The iterative process is stopped once the ray geometry becomes stable : the median of the per-ray maximum perturbations is less than 1 km. We observe this after the 10th iteration, but the final model is only slightly different

TABLE I. – Model geometry for the ARMOR2 inversion. Z is the layer thickness and N is the total number of blocks for each layer. For layers 2 and 3, the cell size is given for the initial geometry, before the irregular discretization.
TABL. I. – *Géométrie de la discrétisation en blocs de la zone cible pour l'inversion des données ARMOR2. Z est l'épaisseur des couches et* N *est le nombre de blocs inversés dans chaque couche. Pour les couches 2 et 3, les dimensions indiquées des blocs sont celles des blocs initiaux, avant la seconde discrétisation irrégulière.*

Layer	EW [km]	NS [km]	Z [km]	N
1	Cones		10	46
2	20	20	20	146
3	25	25	30	160
4	25	25	35	99
5	30	30	35	94
6	30	30	35	108
7	30	30	35	128

from the one computed in the first iteration. This is due to the small amplitude of the velocity perturbations (–3 to +3 %), which are to small to significantly disturb the ray geometry.

In the case of the Armorican Massif, the target volume is divided into 7 layers down to 200 km. The model geometry is given in table I. The topmost layer (layer 1) is a special layer in which one conic pseudo-block is associated to one station. It contains all the rays recorded by the station. The parameters calculated for this layer are difficult to interpret as they reflect very local effects and very short wavelength perturbations. For layers 2 and 3 (10-30 km and 30-60 km, respectively), an uneven discretization has been applied, the block size depending on the ray density. A block initially illuminated by more than 100 rays is vertically divided in four equal blocks. This discretization allows to solve smaller scale structures in the best covered regions, in particular in the Champtoceaux Nappes region.

Seismic anisotropy measurements

Most of the minerals composing the Earth rocks have anisotropic properties. Olivine is of a particular importance for the combined three following reasons : 1) it is the most abundant mineral in the upper mantle; 2) seismic velocity is a significantly anisotropic parameter in olivine; 3) deformed olivine-based aggregates tend to coherently organize their cristallographic lattice. The consequence is that when an olivine-dominated rock is deformed, a lattice preferred orientation (LPO) is developped in the olivine aggregates. It significantly affects seismic wave velocity and can be observed with both body and surface waves. Thus, if one can characterize the LPO from the observation of seismic waves, one can also propose some deformation processes leading to this LPO. Moreover, it is now generally accepted that seismic anisotropy is persistent through time and can be "modified" or "erased" by a new deformation process [e.g. Silver, 1996]. This makes the modeling of anisotropy a powerful tool to help to reconstruct the tectonic history of the Earth.

Xenolith observations [Ben Ismaïl and Mainprice, 1998] together with laboratory experiments [Zhang and Karato, 1995] and numerical modeling [Tommasi, 1998] lead to estimate that LPO in the upper mantle can generate a few percents of seismic velocity anisotropy. In addition, it is possible to link LPO to the direction of deformation : in general, the *a* axis of olivine (high *P* velocity axis) tends to be parallel to the flow direction. As an example, in the case of simple shear, higher velocity is observed parallel to the shear direction. In the case of a pure shear, *a* axis tend to align perpendicularly to the compression direction and thus, higher velocities are observed parallel to the elongation direction. Hence LPO can be characterized by studying seismic anisotropy.

The first studies on seismic anisotropy concerned P_n wave velocities in oceanic lithosphere [Hess, 1964] and then in the continental lithosphere [Bamford, 1977]. These studies are based on the modeling of azimuthal variation of P_n wave velocity propagating horizontally beneath the crust, in the topmost upper mantle. In this case, the anisotropic medium is particularly well located at depth.

Another approach for measuring anisotropy is based on the teleseismic shear wave splitting phenomenum. When a shear wave enters an anisotropic medium, it splits in two quasi-*S* waves which differ in polarization and velocity. Shear waves resulting from the conversion at the core-mantle boundary (*SKS, SKKS, PKS*) are of a particular interest for two reasons : the *P* path in the core removes any previous effect of anisotropy, and the *P* to *S* conversion resulting in *S* wave is vertically polarized (no energy in the transverse direction). Thus, the outgoing wave at the core-mantle boundary is expected to be a pure S_V wave. The observation of energy on the transverse component is thus a clear indication of the presence of an anisotropic layer along the CMB-station path. In the case of an isotropic layer, the particle motion of such an *S*-wave recorded at the station must be linear and parallel to the S_V direction (S_V is perpendicular to the ray and in the ray-plane). If some region visited by the ray is anisotropic, some of the energy is carried by a wave polarized in the S_H direction (S_H is perpendicular to S_V and perpendicular to the ray). As the velocities of the waves differ, the observed particle motion is not linear but elliptical (fig. 3). Several methods [e.g. Bowman and Ando, 1987 ; Silver and Chan, 1991], for a given *S* wave form, allow to describe a candidate anisotropic medium by two and the delay time between the fast and slow waves (written as ϕ and δt, respectively). Some methods taking into account the possibility of multi-layer anisotropic media use the dependance of these parameters on the azimuth and incidence of shear waves to retrieve the anisotropic parameters ϕ and δt in each layer [Bormann *et al.*, 1993 ; Silver and Savage, 1994]. Unfortunately, these approaches require a large number of data and cannot be applied to the data set obtained in the framework of a temporary experiment such as in the present work.

However, we made the choice of modeling our ϕ and δt parameters together with the ray direction as a third parameter. In fact, we compute the fast direction in a plane perpendicular to the ray and thus obtain a ϕ value which is the azimuth of the fast shearwave in this plane. This approach, based on Šílený and Plomerová [1996], allows to describe the anisotropy observation in three dimensions at no cost relative to the classical azimuthal description. It allows to propose a 3D orientation of a simple anisotropic model with a hexagonal symetry which best explains the different observations in different ray directions.

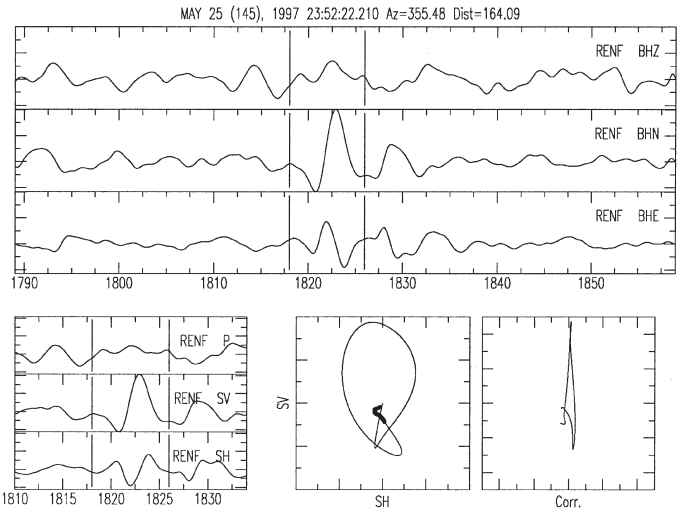

FIG. 3. – Example of an SKKS wave recorded at the broad-band station of Rennes (RéNaSS) for an earthquake originating in the Kermadec Island region. Seismograms are plotted in the *Z,N,E* coordinates system in the top pannel. They are rotated in a coordinates system associated to the ray (P,S_V,S_H) in the bottom pannel. Time is given in seconds since the origin time and the flags limit the signal used for modeling. Particle motions before and after data processing are also represented. One should note that after the correction for anisotropy the particle motion is linear.

FIG. 3. – *Exemple d'enregistrement d'une onde* SKKS *à la station large-bande de Rennes* (RéNaSS) *pour un séisme de la région des îles Kermadec. Les sismogrammes sont représentés en haut dans le système de coordonnées classique* Z,N,E *et dans un système de coordonnées associé au rai* (P,S_V,S_H) *en bas à gauche. Les axes horizontaux sont gradués en secondes depuis l'occurrence du séisme. Le signal exploité est la portion limitée par les marqueurs. Enfin, les mouvements de particule, avant et après correction de l'effet de l'anisotropie, sont tracés respectivement en bas et à droite. On constate un mouvement de particule linéaire après correction.*

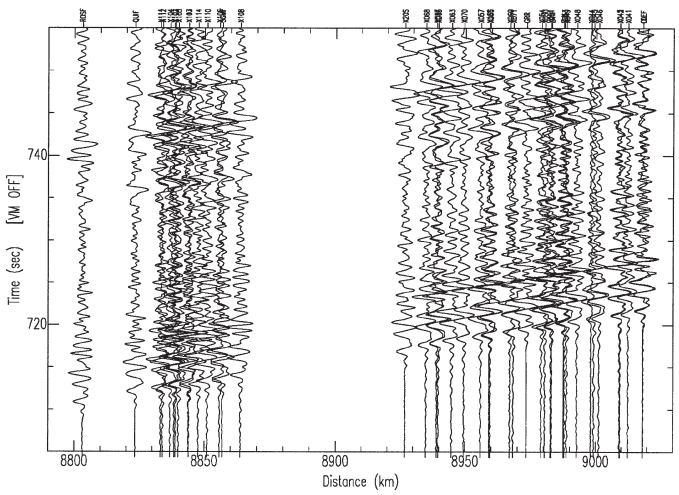

FIG. 4. – Vertical seismograms for an earthquake from Central Mexico (1999/06/15 20:53, 18.4N 97.4W, h = 70 km, mb = 6.4) recorded by the ARMOR2 array. Seismograms are aligned on the *P* onset and sorted with increasing epicentral distance. A band-pass 0.5-3.5 Hz filter has been applied before plotting. The strong coherence of wave forms over a few seconds after the *P* arrival allows the use of a waveform correlation picking method.

FIG. 4. – *Composantes verticales des sismogrammes d'un événement du Centre du Mexique (1999/06/15-20:53, 18.4N 97.4W, h = 70 km, mb = 6.4) enregistré par le réseau* ARMOR2. *Les signaux sont alignés sur l'arrivée de l'onde* P *directe et ordonnés en fonction de la distance épicentrale indiquée en abscisse. En ordonnée, le temps en secondes est relatif à l'heure origine du séisme. Les signaux ont été filtrés entre 0,5 et 3,5 Hz. On remarque la cohérence des formes d'ondes à travers le réseau sur plus de 30 secondes après l'arrivée de l'onde* P. *Cette cohérence est nécessaire sur quelques secondes pour mesurer des temps d'arrivée par une méthode de corrélation de formes d'onde.*

DATA

The temporary arrays were operating from march to december 1997 and from march to august 1999 (see figure 2). The recording sites for the 1997 experiment were selected in order to build two 150 km lines perpendicular to the most important tectonic features. The western line included 17 stations from Saint-Malo to Saint-Nazaire, and the eastern line included 18 stations from Mont Saint-Michel and Pornic. The station spacing is 8 to 10 km and the distance between the lines is about 30 km. In 1999, a supplementary line of 13 stations was installed from Saint-Brieuc to Belle-Ile, about 45 km to the west of the 1997 western line. Moreover, 30 stations were installed east of Nantes, forming a dense 2D array covering the Champtoceaux area. These temporary arrays, together with the permanent stations of the Laboratoire de Detection Géophysique and the Réseau National de Surveillance Sismique form a dense, two dimensions array of 80 stations. In order to take into account the heterogeneity of the recording material and sensors, all the records used in the tomographic study were convolved into a common instrument response (HADES-110 recorder, MarkProduct-L4C sensor), which allows to work with all the seismograms as if they were recorded by the same kind of instrument. Figure 4 shows an example of *P*-wave seismograms after being processed. They are aligned on the *P*-wave arrival time determined with a cross correlation technique, which fixes the upper limit of the picking uncertainty to about 0.1 s. Finally, we applied a regionalized normalization process based on the computation of a reference residual using the stations common to the sub-arrays and the events recorded by these stations [see Judenherc *et al.*, 2001, for the detailed process]. This technique connects the baseline of the different data sets and allows to use the relative residuals from several arrays as if all the stations were operating at the same time.

The final data set for the tomographic problem is made of 5215 travel time residuals associated to 230 events with epicentral distances greater than 30°. The amplitude of the residual variation is about 0.8 s over distances of 250 km. Such variations are significant in the Armorican Massif, as it is usually considered as a relatively stable region.

Teleseismic shear wave splitting measurements have been processed on 23 waveforms of *SKS* waves. This small number of data is due to the low signal to noise ratio resulting from the fact that the period of the microseismic noise is in the same range as that of the teleseismic shear wave period (2-10 s for both). However, a drastic selection process has been applied and we have been able to use 23 high quality records. An example of a record used to compute splitting measurements is shown in figure 3. The elliptical particle motion of the *SKKS* wave is a proof that the wave crossed an anisotropic region between the CMB and the station.

RESULTS

Three dimensionnal P-wave velocity variations

Figure 5 presents the results of the iterative inversion of the travel time residuals after iteration 10. The total number of parameters amounts to 819, considering only the blocks illuminated by at least 10 rays for the inversion. The variance of the residuals before inversion is 0.0552 s^2, and the inversion reduces it by 69 % (down to 0.017 s^2). We present the model as *P*-wave velocity perturbations relative to the reference model. The latter is extracted as a vertical profile from the 3D *S*-wave velocity global model proposed by Woodhouse and Trampert [1995]. *S*-wave perturbations have been converted to *P*-wave perturbations with a division by two according to Souriau and Woodhouse [1985].

The first layer (layer 1, 0-10 km) is not represented as its interpretation is non unique. In the other layers, two vertical domains can be distinguished. The upper domain, down to 130 km, shows an east-west partitioning visible in all three layers (2 to 4). In this domain, the western region

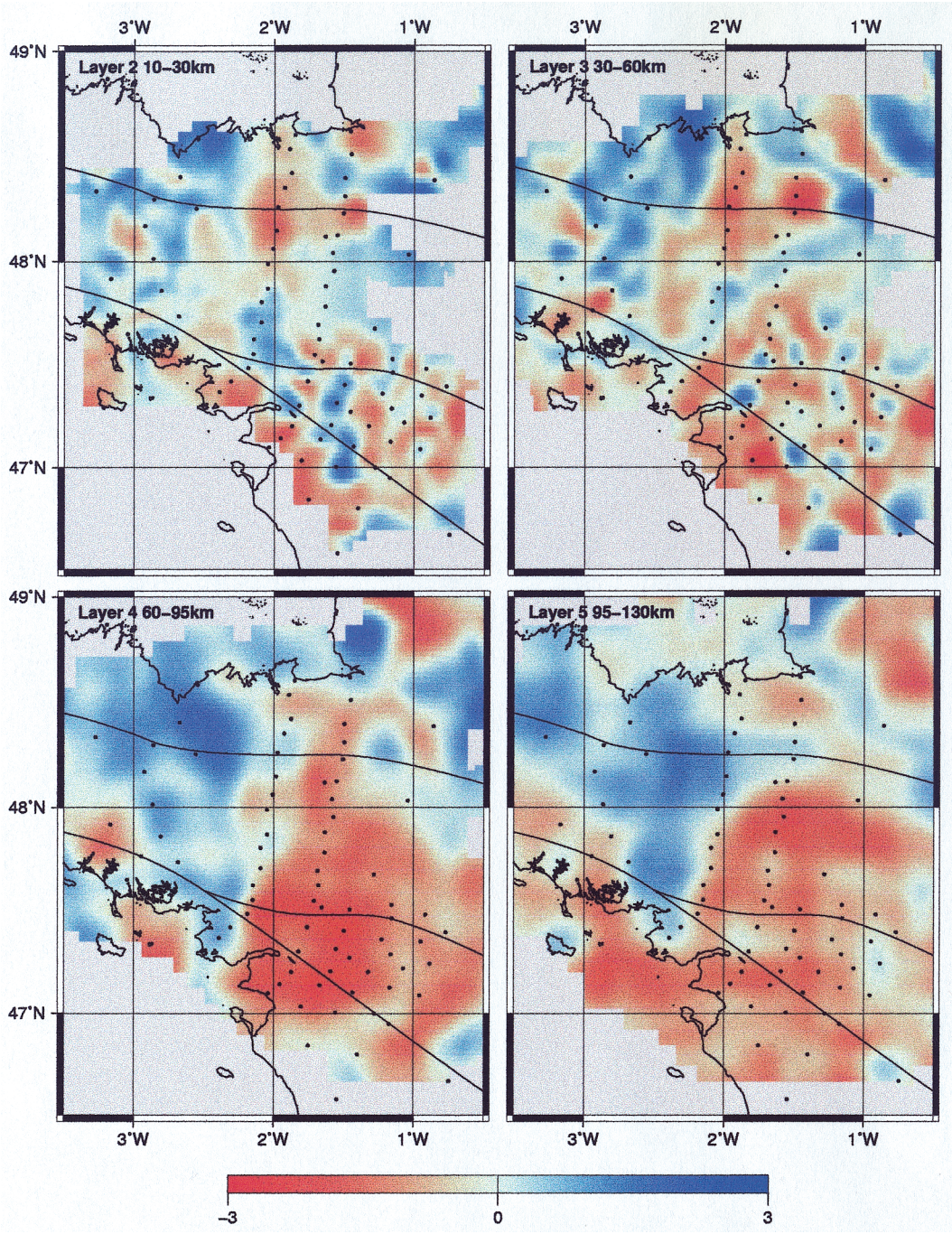

FIG. 5. – *P*-wave velocity perturbations in % for layers 2 to 7 after the iterative inversion of the ARMOR2 data set. Red colors indicate negative velocity pertubations while blue colors indicate positive velocity perturbations.
FIG. 5. – *Perturbations de la vitesse des ondes* P *en % pour les couches 2 à 7 résultant de l'inversion itérative du jeu de données ARMOR2. Le rouge indique des perturbations de vitesse négatives tandis que le bleu indique des perturbations de vitesse positives.*

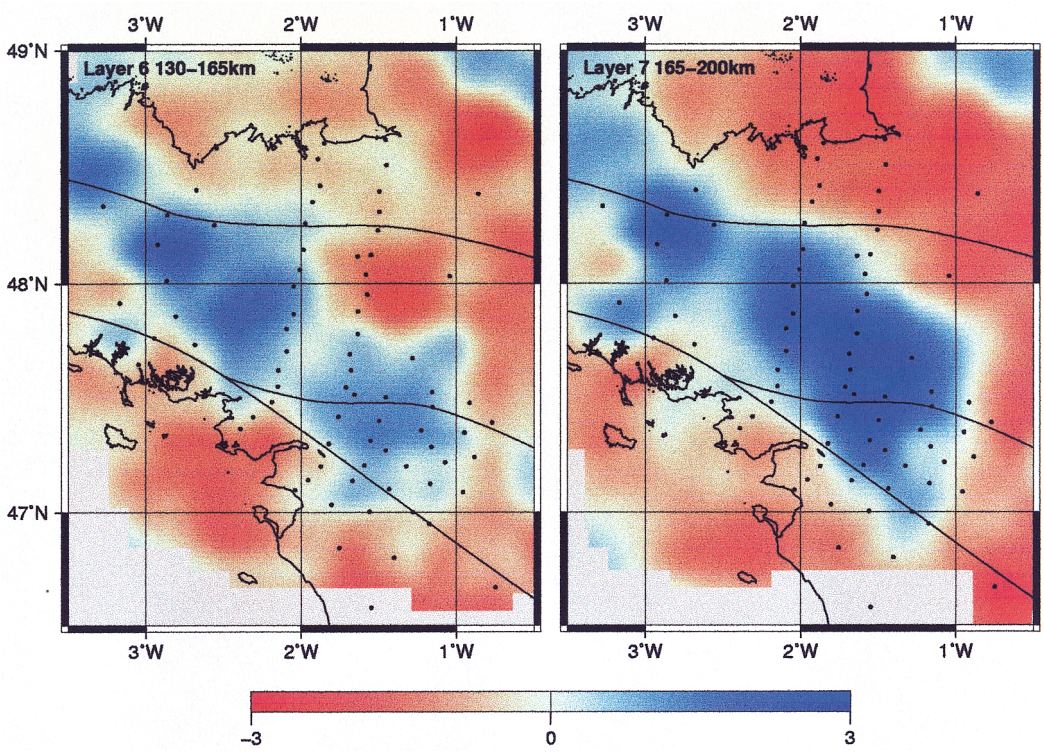

FIG. 5. – continued -- *suite*

is characterized by positive anomalies, whereas a wide negative anomaly is observed in the SE region. One should note that the North Armorican Shear Zone does not appear as a major feature in the velocity model. The same is true for the Champtoceaux Nappes : no clear signature of fast (and so presumably heavy) body can be seen in the upper layer. At the depth of 130 km, corresponding to the boundary between layer 4 and layer 5, a dramatic change of the structure geometry is observed. Velocity perturbations are organized in three NW-SE elongated areas : *P*-wave velocity is low to the south, high in a 70 km wide central area and low again in the northern area. The northern and southern boundaries of the high velocity central body are linear and oriented parallel to the South-Armorican Shear Zone.

Seismic anisotropy of P_n-waves and *SKS*-waves

All the results are displayed together in figure 6. The P_n anisotropy has been extracted from a larger model computed for the whole of France [Judenherc *et al.*, 1999]. Fast directions are oriented E-W, parallel to the North Armorican Shear Zone in the northern part of the Armorican Massif and NW-SE, parallel to the South-Armorican Shear Zone, in the southern part of the AM. The amplitude of the anisotropy is 3 to 4 %. The strong correlation between the P_n-wave fast directions and the direction of NASZ and

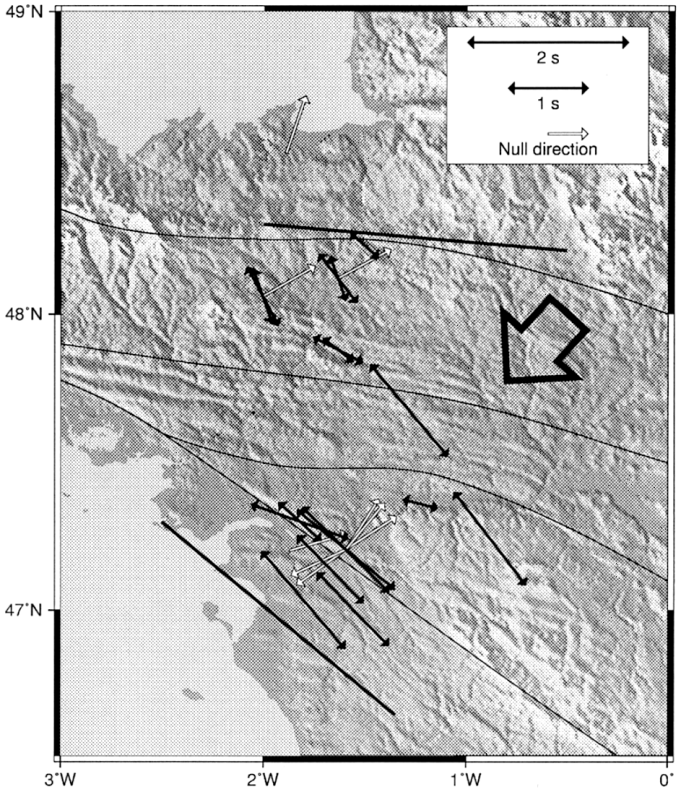

FIG. 6. – Results of body wave anisotropy measurements in the Armorican Massif. The magnitude of the P_n velocity anisotropy is 3 to 4%, the fast directions are represented by the two long lines. The black double-arrows are parallel to the azimuth of the fast *SKS* direction (ϕ) and their length is proportional to the delay δt between the fast and slow waves. The white arrows indicate the azimuth of events associated to the observation of null directions. The big arrow shows the absolute plate motion of the European plate following the HS2-Nuvel1 model [Gripp and Gordon, 1990].
FIG. 6. – *Synthèse des résultats des mesures d'anisotropie des ondes de volume dans le Massif armoricain. L'anisotropie de vitesse de propagation des ondes P_n est de 3 à 4%, les directions rapides sont représentées par les deux longs traits. Les doubles-flèches noires sont orientées dans l'azimut de la direction rapide ϕ et leur longueur est proportionnelle au délai δt mesuré aux différentes stations. Les flèches blanches simples indiquent l'azimut des séismes associés aux directions nulles. La flèche à droite indique le mouvement absolu de la plaque Eurasie dans le modèle HS2-Nuvel1 [Gripp and Gordon, 1990].*

SASZ suggests that the deformation might be coherent within the crust (where the deformation is marked by the fault zones), down to the P_n-wave propagation layer in the topmost upper mantle just beneath the crust (where deformation is represented by the fast P_n directions).

Teleseismic shear wave splitting measurements also show fast directions parallel to the SASZ in the southern part of the region. This NW-SE direction remains quite stable accross the whole AM. We cannot see any correlation with the NASZ in the northern part of the AM as it is observed for the P_n anisotropy. Close to the SASZ and to the south of the SASZ, the delay times (δt-values) are larger (about 1.25 s) than to the north. If we consider a single anisotropic layer with an anisotropy rate of about 3 % for the *S*-wave velocity [Mainprice and Silver, 1993], these delays indicate a thickness of 120 to 130 km. In the northern part, where the delay times are smaller, a value of about 80 km is proposed according to the same rule of thumb.

DISCUSSION

Some recent works discuss the validity of the basic hypotheses of the tomographic method and their consequences on the velocity model. In particular, the effect of the velocity perturbations located outside of the target volume has been estimated by Masson and Trampert [1997]. These velocity perturbations, located in the deep upper mantle and in the lower mantle, are considered to be of long wave length and of small amplitude. Consequently, their effect on the observed travel time residual is expected to be smooth. The computations of Masson and Trampert show a maximum contribution of 0.5 s along an 800 km profile. As the source of those perturbations is deep, a monotonous shape is observed along the profile. Thus, as the maximum extension of the Armorican array is about 300 km, one can rule out the off-target volume velocity perturbations as a significant contribution to our observed residuals.

The bias due to anisotropic structures has also been estimated by Sobolev *et al.* [1999] who conclude that both anisotropic structure geometry and ray geometry control the bias. We have thus tested some realistic configurations based on the modeling of our anisotropy measurements (see sections 4.2 and 5.2). The inversions of synthetic data sets computed with anisotropic models show that the bias is related to the change of the anisotropy pattern rather than to the shape of the anisotropic structures [see Judenherc, 2000, for detailed results]. Generally, we observe that the maximum velocity perturbation output from a 3 % anisotropy input is about 1 % and that the shapes of those velocity images do not resemble the maps obtained from the inversion of real data. It is thus concluded that while an anisotropy bias exists, it is of a second order effect in the velocity images.

Resolution

The question of the accuracy of the computed model is raised by any tomographic problem. In this work, we solve the following linear problem : d = Gm, where d represents the observations (normalized residuals) and m represents the model vector (slowness perturbations). The matrix G describes the direct problem. By using a least square approach, the computed resolution matrix R is defined as the product LG where L is the inversion operator. The resolution matrix is defined by the ray geometry and the model parameterization. It defines the way we "see" the actual Earth with our theory and data set. Thus, if m_0 represents the actual Earth according to a given parameterization, the ray geometry associated to the resolution matrix R allows to compute a model $\hat{m}$ which equals the product Rm_0. A given coefficient *i, j* of the R matrix represents the trade-off between parameters *i* and *j*. Consequently, one tries to get a resolution matrix as close as possible to the identity matrix. In the ideal case, each parameter is fully retrieved (the value of the diagonal terms is one) and shows no correlation with any other parameter (each off-diagonal term is null). The whole resolution matrix is represented in figure 7. The diagonal terms are quite large (70 % are greater than 0.70) and off-diagonal terms are small (maximum value is 0.18). The amplitudes observed on the secondary diagonal lines represent the trade-off between blocks in different layers. One should note that the shape of the matrix for each layer depends on the block numbering which can be irregular as we applied an irregular parameterization in the upper layers. The negative terms close to the diagonal indicate that a block is slightly anti-correlated with its neighbouring blocks, but their amplitude is generally low (less than 0.2).These general observations on the resolution matrix indicate that our model is robust, and that the observed trade-off is only a second order effect.

However, since it is difficult to link the resolution matrix with the block geometry of the study area, we mapped the diagonal terms of the resolution matrix in figure 8. If we consider that a value greater than 0.5 is a threshold value above which the model is reliable, we must consider that for the crustal layer, only the Champtoceaux Nappes region is well resolved. For the deeper layers, the whole area covered by the array of stations can be considered as well resolved.

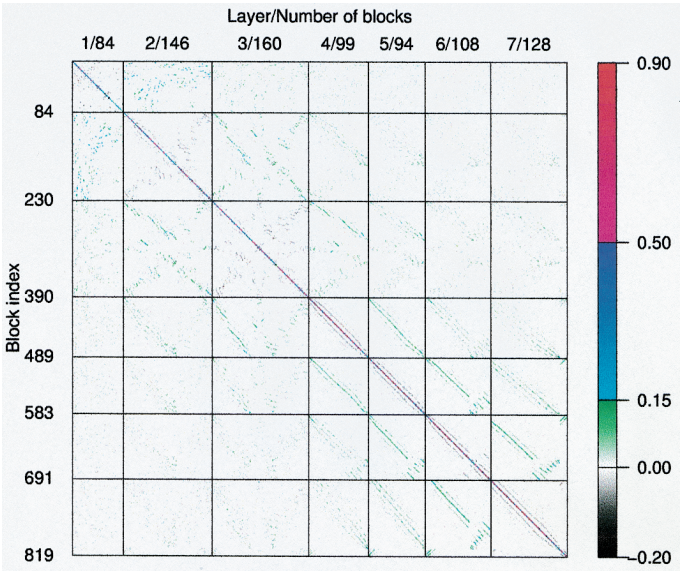

FIG. 7. – Full resolution matrix associated with the tomographic inversion of the ARMOR2 data set. Left axis labels correspond to the cell index. The layer index and the number of cells in each layer are indicated on the top axis.

FIG. 7. – *Matrice de résolution associée à l'inversion linéaire des données ARMOR2. Les axes sont gradués en indice de bloc. Les numéros de chaque couche et le nombre de blocs par couche sont indiqués sur l'axe supérieur.*

Orientation and localisation of anisotropy

Figure 6 shows the fast directions as deduced from the analysis of shear-wave splitting measurements, detailed results being given in table II. We also represent the null-directions which indicate the azimuth of earthquakes for which a clear *SKS* wave was observed but no elliptical particle motion. According to the hypothesis of a single anisotropic layer characterized by a hexagonal symetry system, these observations are possible only if the *SKS*-wave propagates in a direction close to the symetry axis and/or if the wave is polarized in the symetry plane of the medium. In such cases, the incident wave always shows a linear particle motion parallel to one of the symetry axes or planes of the medium. Null-directions should thus be observed parallel or perpendicular to the fast directions. In figure 6, null directions are oriented NE and SW in the south of the Armorican Massif and NE in the north. However, data 1 and 12 (see table II) recorded at the broad-band station of Rennes are not compatible with a medium characterized by a horizontal hexagonal symetry axis. In the case of this simple model, the observation of a N061°E null-direction (data 12) should be correlated to the observation, at the same station, of a null-direction in the opposite direction. This is not observed for data 1, which shows a clear elliptical particle motion from azimuth N237°E (fig. 9). These observations are however compatible if one considers an inclined hexagonal symetry axis. The method proposed by Šílený and Plomerová [1996] allows to determine the 3D orientation of the symetry axis. For all the results in the north of the Armorican Massif, this method gives a N057°E axis dipping 34° to the NE, *i.e.* a SW dipping foliation plane. With a thickness of 80 km as deduced from the average δt (0.8 s) and with a 3 % anisotropy amount, the theoretical delays for data 1 and 12 are respectively 0.7 s and 0.11 s. The δt associated to data 12 (0.11 s) cannot be properly measured and we observe a null direction.

In the south of the massif, with the exception of data 13 and 24 which appear to be outliers, the null-directions and the fast directions are mostly compatible with a simple model with a horizontal hexagonal symetry axis. Moreover, a remarkable correlation between the direction of the SASZ, the P_n fast direction, and the teleseismics hear wave fast direction can be observed. These observations suggest a vertically coherent deformation from the crust down to about 130 km, considering a 3 % anisotropy amount. In this case, the anisotropy recorded by the *SKS*-waves would be explained by a single 130 km layer. If the anisotropic medium was thicker than 200-250 km for example, the observations would be more homogeneous at the scale of the Armorican Massif. Measurements are clearly separated in two groups : in the north, delays are small and can be explained by an NE dipping anisotropy pattern (SW dipping foliation) while in the south, the δt values are 0.4 s larger and can be explained by a simple medium with a horizontal hexagonal symetry axis (vertical foliation). The boundary between the two groups cannot be clearly located but the change occurs within less than 70 km. This is again in favour of a shallow (lithospheric rather than asthenospheric) anisotropic layer. Moreover, the observation of two distinct groups rules out the absolute plate motion (APM) as a cause of the anisotropy, since in this case the anisotropy should be very homogeneous at the scale of the Armorican Massif. We also observe a high angle (80 to 90°) between the fast directions and the APM of the European plate according to the model proposed by Gripp and Gordon [1990]. Even if the APM is not well constrained because of the small velocity of the European plate, it is probably not the cause of the anisotropy.

TABLE II. – Shear wave splitting measurements obtained in the Armorican Massif. Results are given as the delay between the fast and slow shear waves and the polarization vector of the fast shear wave. This vector is defined by two angles : the azimuth ϕ and the incidence θ, positive upward. We also give the location and origin time of the used earthquakes.
TABL. II. – *Synthèse des mesures de biréfringence des ondes S télésismiques. Les résultats sont représentés par le délai entre l'onde rapide et l'onde lente* (δt) *et la direction de polarisation de l'onde rapide décrite par deux angles : l'azimut* ϕ *de la direction rapide et l'angle* θ *qui est mesuré entre la direction de polarisation de l'onde rapide et la verticale, compté positivement vers le haut. Sont données également l'heure origine et les coordonnées des événements utilisés.*

	Sta.	Az.	Dist.	ϕ	θ	δt	Origin time	Lat.	Long.	Depth
1	RENF	236	90	161	94	0.6	1997.01.23-02.15.22	–22.0	–65.7	276
2	X22H	18	142		Linear		1997.04.21-12.02.26	–12.6	166.7	33
3	X09L	18	151	–52	95	0.5	1997.05.21-14.10.26	–20.4	169.3	57
4	X15H	18	152	–48	96	0.7	1997.05.21-14.10.26	–20.4	169.3	57
5	X27H	17	151	–19	101	0.7	1997.05.21-14.10.26	–20.4	169.3	57
6	RENF	355	164	142	102	0.8	1997.05.25-23.22.33	–32.1	179.8	332
7	X05L	356	163	313	99	0.5	1997.05.25-23.22.33	–32.1	179.8	332
8	X09L	355	164	298	97	0.7	1997.05.25-23.22.33	–32.1	179.8	332
9	X15H	354	164	290	95	1.3	1997.05.25-23.22.33	–32.1	179.8	332
10	X27H	354	164	332	102	0.8	1997.05.25-23.22.33	–32.1	179.8	332
11	X17H	73	126		Linear		1997.08.10-09.20.30	–16.0	124.3	10
12	RENF	61	120		Linear		1997.09.26-15.48.34	–5.4	129.0	253
13	NAF	234	100		Linear		1998.07.29-07.14.24	–32.3	–71.3	51
14	NAF	56	110		Linear		1998.09.02-08.37.29	5.4	126.8	50
15	NAF	244	88		Linear		1998.10.08-04.51.42	–16.1	–71.4	136
16	NAF	39	91		Linear		1999.01.24-00.37.04	30.6	131.1	33
17	X040	34	98	140	92	1.5	1999.07.03-05.30.10	26.3	140.5	430
18	X042	34	98	143	93	1.5	1999.07.03-05.30.10	26.3	140.5	430
19	X052	34	98	104	87	0.4	1999.07.03-05.30.10	26.3	140.5	430
20	X057	33	99	136	92	1.2	1999.07.03-05.30.10	26.3	140.5	430
21	X070	33	99	140	92	1.6	1999.07.03-05.30.10	26.3	140.5	430
22	X071	34	99	136	92	1.3	1999.07.03-05.30.10	26.3	140.5	430
23	NAF	33	103		Linear		2000.03.28-11.00.19	22.4	143.6	116
24	NAF	230	93	135	91	1.5	2000.04.23-17.01.17	–28.4	–62.9	609
25	NAF	29	90	129	92	1.6	2000.07.20-18.39.19	36.6	141.0	49

INTERPRETATION

Seismic velocity variations are usually interpreted as the consequence of thermal or chemical variations. These two causes are not incompatible. In recently active areas, invoking thermal anomalies only is sufficient to explain most of the modelled velocity perturbations as in the French Massif Central [Granet *et al.*, 1995 ; Sobolev *et al.*, 1996]. However, since the Armorican Massif is tectonically stable since more than 250 m.y., it seems unlikely to link the velocity perturbations to a thermal anomaly only. In particular, the central positive anomaly located between 130 and 200 km is limited to the north and to the south by some velocity change from +2 % to –2 % in less than 30 km. If we accept that the bias due to unmodelled anositropy is less than 1-1.5 %, more than 2.5 % must be explained by thermal or compositional changes. If we then consider a conversion factor of 100°/% [e.g. Sobolev et al., 1997], the thermal anomaly associated to the velocity changes would exceed 250°C. Such high thermal perturbations should be correlated to a high heat flow which is not the case in this area [Vasseur, 1982].

These observations suggest that the velocity perturbations are most likely of chemical or compositional origin. Then, the question of considering the Armorican Massif as the collage of lithospheric units of different natures and dif-

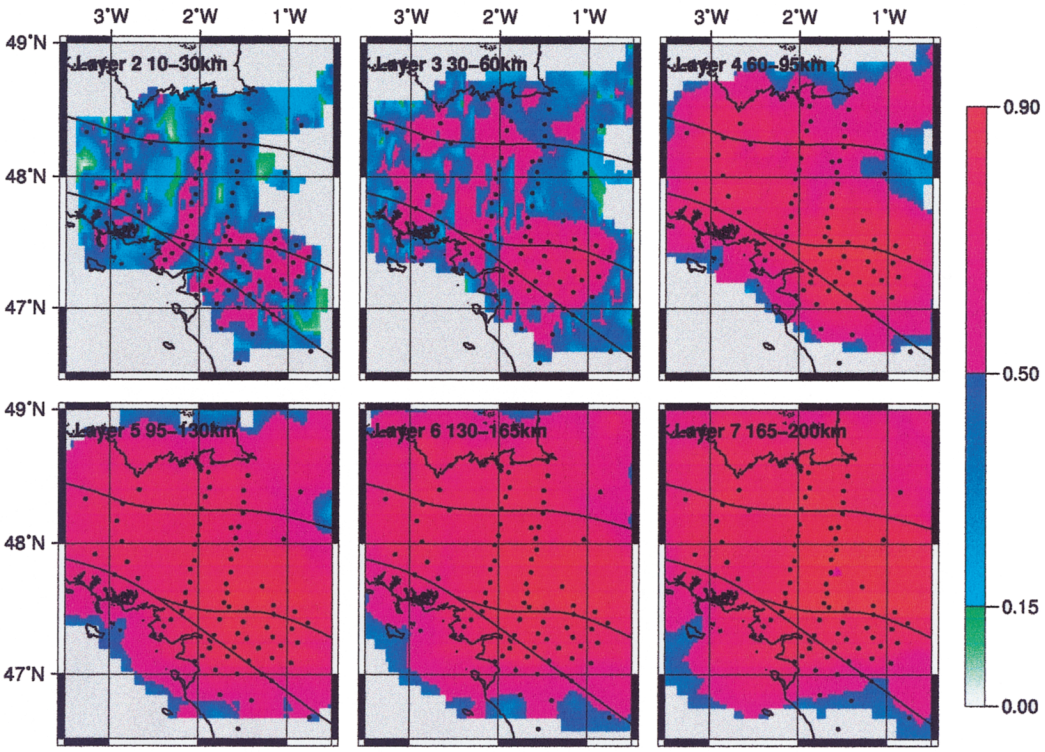

FIG. 8. – Diagonal terms of the resolution matrix associated with the tomographic inversion of the ARMOR2 data set. The first layer is not represented. Black dots indicate the station location. The color scale is the same as for figure 7.
FIG. 8. – *Termes diagonaux de la matrice de résolution associée à l'inversion des données ARMOR2. La première couche (les « cônes ») n'est pas représentée. Les points noirs localisent les sites d'enregistrement. L'échelle de couleur est la même que dans la figure 7.*

ferent origins arises. The teleseismic shear wave splitting measurements show at least two distinct domains which recorded different ancient deformation events. We propose to interpret the body wave fast directions as reflecting the lithospheric fabric produced by a deformation event [e.g. Silver, 1996]. In the south of the Armorican Massif, the lithospheric fabric can be associated with the Carboniferous transpressive regime along the SASZ i.e. according to this hypothesis, it can be considered as a Hercynian fabric. This is supported by the remarkable correlation bewteen the *Pn* fast directions, the *SKS* fast directions and the maximum shear direction indicated by the SASZ. Such a vertical consistency cannot be observed in the north of the CAD and NAD. On the one hand, the *Pn* direction indicates a coupling between the crustal Hercynian deformation and the deformation of the topmost upper mantle. On the other hand, the fabric determined by the shear-wave splitting measurements is not compatible with Hercynian deformations, since it makes a 30° angle with the Hercynian trend. The origin of this inclined and oblique fabric is probably of Cadomian age. The topmost upper mantle and the deeper lithospheric mantle must be separated by a decoupling level in order to explain the fast rotation of P_n fast directions.

The integration of all the above arguments lead to suggest a northern dipping subduction process which occurred just before the continental subduction at the location of the SASZ (figure 10). Accordingly, the central positive anomaly detected between 130 and 200 km would correspond to a preserved remnant of the subducted lithosphere. This lithosphere, belonging to a pre-Hercynian block, is characterized by a *P*-wave velocity higher than in the lithosphere to the

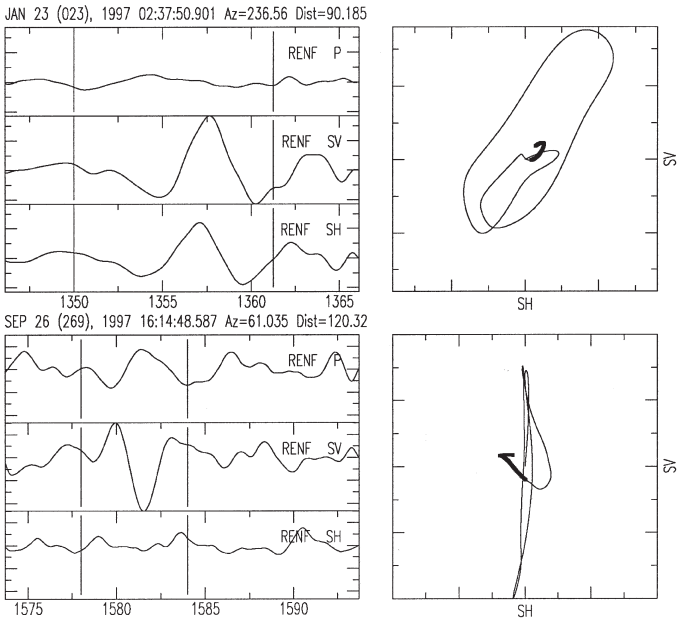

FIG. 9. – Teleseismic shear waves recorded at the broad-band station of Rennes and associated with two events with opposite azimuth. On the top panel (observation 1 in table II), the particle motion shows an elliptical shape in the *SV, SH* (ray related) coordinate system. On the bottom panel (observation 12), the particle motion is linear.
FIG. 9. – *Signaux enregistrés à la station large bande de Rennes et associés à deux formes d'ondes* S *télésismiques dont les azimuts sont opposés. En haut (donnée 1 du tableau II) le mouvement de particule est elliptique dans le repère* SV, SH. *En bas (donnée 12), le mouvement de particule est linéaire.*

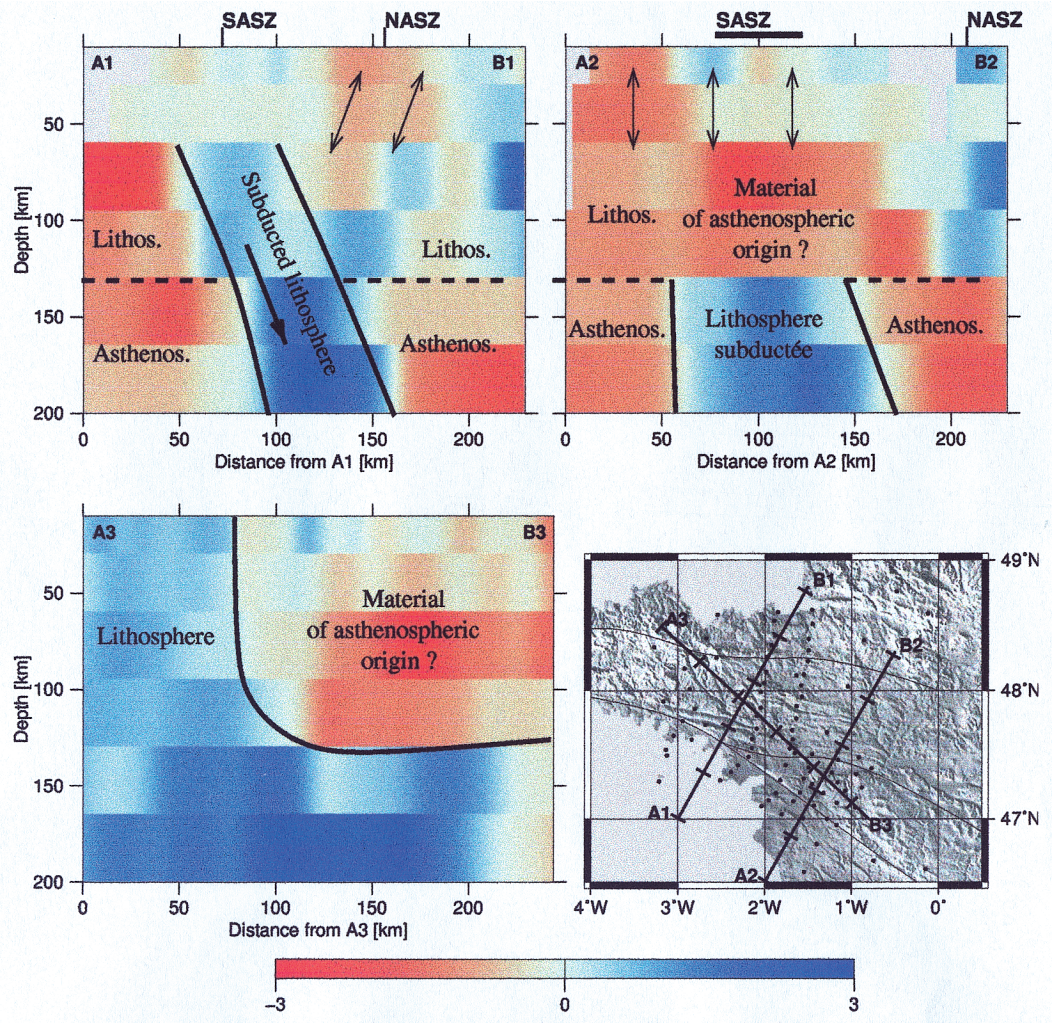

FIG. 10. – Interpretation of cross-sections deduced from the ARMOR2 3D velocity model. These cross-sections are computed along the profiles represented on the map (bottom right pannel). They represent the velocity perturbations low-passed filter by a gaussian function with a width equaling the smallest cell in each layer. The south and north armorican shear zones are located on the top of cross-sections A1B1 and A2B2. All the images are drawn with the same scale, without vertical exaggeration. The double arrows represent the orientation of the lithospheric fabric as deduced from the shear wave splitting analysis.

FIG. 10. – *Interprétation des coupes extraites du modèle de vitesse tridimensionnel ARMOR2. Ces coupes sont calculées le long des lignes représentées sur la carte en bas à droite. Elles représentent les variations de vitesse filtrées par une fonction gaussienne dont la largeur est égale à la plus grande dimension latérale des blocs dans chaque couche. Les Cisaillements sud- et nord-armoricains sont repérés en haut des coupes A1B1 et A2B2. Toutes les coupes sont à la même échelle, sans exagération verticale. Les double-flèches représentent l'orientation de la fabrique déduite de l'analyse de la biréfringence des ondes* S *télésismiques*.

north, which is probably of Cadomian origin. In this geodynamic scenario, the low velocity body located in the southeastern part of the Armorican Massif down to 130 km is probably younger than the subduction event (Ordovician-Silurian) as it affects the subducted lithosphere (profile A2B2, fig. 10). This anomaly is also probably of a pre-Carboniferous age, as the anisotropy in the lithosphere in the south of the Armorican Massif, is attributed to the transpressive phase of Carboniferous age.

Finally, the lithosphere-asthenosphere boundary (LAB) can be seismologically defined, according to Kissling and Spakman [1996], by the depth at which the vertical velocity gradient becomes negative. The presented tomographic images do not allow to determine this depth as the vertical gradient strongly depends on the reference model. However, several observations indicate a possible transition at the 130 km depth. This depth is obviously related to the model geometry but some inversion tests processed with various layer thicknesses have shown that the 130 km depth is the most appropriate for the problem. Taking into account the vertical resolution and the model thickness of each layer at this depth, an uncertainity of about ± 15 km for the depth of the LAB has to be considered. Important first order changes can be observed at that depth : in the upper domain, velocity perturbations exhibit an E-W partitionning; they are organized in three NW-SE elongated areas in the lower domain. In addition, as previously explained, considering a 3 % anisotropy amount, this depth of 130 km could correspond to the base of the anisotropic layer in the south of the Armorican Massif.

CONCLUSIONS

Seismological tools applied to the Armorican Massif emphasize the different nature and origin of several collated lithospheric blocks. Considering this tectonically and ther-

mally stable region, the lateral velocity changes must be interpreted mainly in terms of compositional changes. Seismic anisotropy mapped in the lithosphere results from two ancient tectonic events : the Hercynian deformation in the south, along the South-Armorican Shear Zone, and probably a Cadomian deformation in the north. The combined interpretation of anisotropy measurements and velocity tomography imaging applied to the same object reveals the signatures of two successive Hercynian collision stages : a northward subduction followed by a strong transpressive regime. The latter event inprinted the South-Armorican lithosphere fabric differently from the older North-Armorican lithosphere.

The deep crustal tomographic model does not allow to identify any clear signature related to the Champtoceaux Nappes, even if this region is probably well-resolved. Also, no correlation between the North Armorican Shear Zone and the tomographic model or the teleseismic shear wave splitting measurements can be observed. Neither the NASZ, nor the Champtoceaux Nappes do significantly affect the Armorican lithosphere. Thus, the only major geological structure in the Armorican Massif is the South Armorican Shear Zone whose influence can be detected down to the base of our model at 200 km. The imaging of old structures related to the Hercynian collision down to great depths shows that such an important geodynamic event as continental collision must be considered at the lithospheric or litho-asthenospheric scale. These results also reveal the limits of a strictly thermal interpretation of litho-asthenospheric tomographic images as this approach would lead to unrealistic thermal anomalies for the Armorican Massif.

Acknowledgements. – The authors thank A. Vauchez and an anonymous reviewer for their suggestions and improvements on a former version of the manuscript. We also thank all the people who contributed to the installation of the arrays. This work has been supported by the GéoFrance-3D project.

References

Aki K., Christofferson A. & Husebye E.S. (1977). – Determination of the three-dimensional seismic structure of the lithosphere. – *J. Geophys. Res.*, **82**, 277-296.

Auvray B. (1977). – Genèse et évolution de la croûte continentale dans le nord du Massif armoricain. – Thèse Sci., Univ. Rennes.

Balé P. & Brun J.P. (1986). – Les complexes métamorphiques du Léon (NW Bretagne) ; un segment du domaine éo-hercynien sud armoricain translaté au Dévonien. – *Bull. Soc. géol. Fr.* (8), **VIII**, 471-477.

Ballèvre M., Bosse V. & Gapais D. (2000). – L'isograde du grenat dans les schistes bleus de l'île de Groix (Bretagne méridionale) : une zone de cisaillement rétrograde. – *18e R S T*, livre en dépôt à la SGF.

Bamford D. (1977). – P_n velocity anisotropy in a continental upper mantle. – *Geophys. J.R. Astron. Soc*., **49**, 29-48.

Ben Ismaïl W. & Mainprice D. (1998). – An olivine fabric database : an overview of upper mantle fabrics and seismic anisotropy. – *Tectonophysics*, **296**, 145-157.

Bonnet S. (1998). – Tectonique et dynamique du relief : le socle armoricain au Pléistocène. – Thèse Sci., Géosciences Rennes, Université de Rennes I.

Bormann P., Burghardt P.T., Makeyeva L.I. & Vinnik L.P. (1993). – Teleseismic shear-wave splitting and deformations in Central Europe. – *Phys. Earth Planet. Int.*, **78**, 157-166.

Bosse V., Féraud G. & Ballèvre M. (2000). – Géochronologie des roches éclogitiques du Complexe de Champtoceaux (Massif armoricain, France) : cohérence des méthodes U-Pb, Sm-Nd, Rb-Sr et ^{40}Ar-^{39}Ar. – *18e R S T*, Livre en dépôt à la SGF.

Bowman J.R. & Ando M. (1987). – Shear-wave splitting in the upper-mantle wedge above the Tonga subduction zone. – *Geophys. J. R. Astron. Soc.*, **88**, 25-41.

Brown M. & Dallmeyer R.D. (1996). – Rapid Variscan exhumation and the role of magma in core complex formation : southern Brittany metamorphic belt, France. – *J. Metam. Geol.*, 361-379.

Brun J.-P., Ballard J.-F. & Le Corre C. (1991). – Identification of Ordovician block-tilting in the Hercynian fold belt of Central Brittany (France) : field evidence and computer models. – *J. Struct. Geol.*, **13**, 419-429.

Chantraine J., Autran A. & Cavelier C. (1996). – Carte géologique de la France à 1/1000.000. – Ed. BRGM.

Cogné J. & Wright A.E. (1980). – L'orogène Cadomien. – Geology of Europe from Precambrian to the post-Hercynian sedimentary basins. – *26th International Geological Congress. – BRGM Mem.*, **108**, 29-55.

Franklin J.N. (1970). – Well-posed stochastic extension of ill-posed linear problems. – *J. Math. Anal. Appl*., **31**, 682-716.

Gapais D., Lagarde J.-L., Le Corre C., Audren C., Jegouzo P., Casas SINZ A. & Van Den Driessche J. (1993). – La zone de cisaillement de Quiberon : témoin d'extension de la chaîne varisque en Bretagne méridionale au Carbonifère. – *C.R. Acad. Sci.,* Paris, **316**, 1123-1129.

Granet M., Wilson M. & Achauer U. (1995). – Imaging a mantle plume beneath the Massif Central (France). – *Earth Planet. Sci. Lett.*, **17**, 1109-1112.

Graviou P. & Auvray B. (1985). – Caractérisation pétrogaphique et géochimique des granitoïdes cadomiens du domaine nord-armoricain : implications géodynamiques. – *C.R. Acad. Sci.*, Paris, **301**, 315-318.

Gripp A.E. & Gordon R.G. (1990). – Current plate velocities relative to the hotspots incorporating the NUVEL-1 global plate motion model. – *Geophys. Res. Lett.*, **17**, 1109-1112.

Guiraud M., Burg J.P. & Powell R. (1987). – Evidence for a Variscan suture zone in the Vendée, France; a petrographical study of blueschist facies rocks from Bois de Cené. – *J. Metam. Geol.*, **5**, 225-237.

Hess H.H. (1964). – Seismic anisotropy of the uppermost mantle under oceans. – *Nature*, **203**, 629-630.

Judenherc S. (2000). – Etude et caractérisation des structures hercyniennes à partir de données sismologiques : le cas du Massif armoricain. – Thèse Sci., Université Louis Pasteur, Strasbourg I, Strasbourg.

Judenherc S., Granet M. & Boumbar N. (1999). – Two-dimensional anisotropic tomography of lithosphere beneath France using regional arrival times. – *J. Geophys. Res.*, **104**, 13201-13215.

Judenherc S., Granet M., Brun J.P., Poupinet G., Plomerová J., Mocquet A. & Achauer U. (2001). – Images of lithospheric heterogeneities in the Armorican segment of the Hercynian range in France. – *Tectonophysics* (sous presse).

Kissling E. & Spakmann W. (1996). – Interpretation of tomographic images of uppermost mantle structure ; examples from the western and central Alps. – *J. Geodyn*., **21**, 97-111.

Lenôtre N., Thierry P., Blanchin R. & Brochard G. (1999). – Current vertical movement demonstrated by comparative levelling in Brittany (northwestern France). – *Tectonophysics*, **301**, 333-344.

Mainprice D. & Silver P.G. (1993). – Interpretation of *SKS*-waves using samples from the subcontinental lithosphere. – *Phys. Earth Planet. Inter.,* **78**, 257-280.

MASSON F. & TRAMPERT J. (1997). – ACH or how reliable is regional teleseismic delay time tomography. – *Phys. Earth Planet. Inter.,* **102**, 21-32.

ŠÍLENÝ J. & PLOMEROVÁ J. (1996). – Inversion of shear-wave spliting parameters to retrieve three-dimensional orientation of anisotropy in continental lithosphere. – *Annu. Rev. Earth Planet. Sci.*, **95**, 277-292.

SILVER P.G. (1996). – Seismic anisotropy beneath the Continents : probing the depth of geology. – *Annu. Rev. Earth Planet. Sci.,* **24**, 385-432.

SILVER P.G. & CHAN W.W. (1991). – Shear wave splitting and subcontinental mantle deformation. – *J. Geophys Res*., **96**, 16429-16454.

SILVER P.G. & SAVAGE M.K. (1994). – The interpretation of shear-wave splitting parameters in the presence of two anisotropic layers. – *Geophys. J. Int*., **119**, 949-963.

SOBOLEV S., GRÉSILLAUD A. & CARA M. (1999). – How robust is isotropic delay time tomography for anisotropic mantle ? – *Geophys. Res. Lett.*, **26**, 509-512.

SOBOLEV S.V., ZEYEN H., GRANET M., ACHAUER U., BAUER C., WERLING F., ALTHERR R. & FUCHS K. (1997). – Upper mantle temperatures and lithosphere-asthenosphere system beneath the French Massif Central constrained by seismic, gravity, petrologic and thermal observations. – *Tectonophysics*, **275**, 143-164.

SOBOLEV S.V., ZEYEN H., STOLL G.,WERLING F., ALTHERR R. & FUCHS K. (1996). – Upper mantle temperatures from teleseismic tomography of the French Massif Central including effects of composition, mineral reactions, anharmonicity, anelasticity and partial melt. – *Earth Planet. Sci. Lett.*, **139**, 147-163.

SOURIAU A. & WOODHOUSE J. (1985). – A worldwide comparison of predicted S-wave delays from a three dimensional upper mantle model with P-wave station corrections. – *Phys. Earth Planet. Inter.*, **39**, 75-78.

STECK L.K. & PROTHERO W.A. (1991). – A 3-D raytracer for teleseismic body-wave arrival times. – *Bull. Seismol. Soc. Am.*, **81**, 1332-1339.

TOMMASI A. (1998). – Forward modeling of the development of seismic anisotropy in the upper mantle. – *Earth Planet. Sci. Lett.*, **160**, 1-13.

VASSEUR G. (1982). – Synthèse des résultats de flux géothermique en France. – *Ann. Geophys.*, **38**, 189-201.

VERGNE J. (1998). – Un outil de tomographie télésismique robuste très utilisé et critiqué : la méthode ACH. Analyse critique et améliorations. – Mémoire de DEA, EOST, Université Louis Pasteur, Strasbourg I.

WESSEL P. & SMITH W.H.F. (1995). – New version of the generic mapping tools released. – *EOS, Trans. Am. geophys. Un.*, **76**, 329.

WOODHOUSE J. & TRAMPERT J. (1995). – Global upper mantle structure inferred from surface wave and body wave data. – *EOS, Trans. Am. geophys. Un.*, **76**, 422.

ZHANG S. & KARATO S.I. (1995). – Lattice preferred orientation of olivine aggregates deformed in simple shear. – *Nature*, **375**, 774-777.